Trends in Analytical Chemistry 152 (2022) 116618

Contents lists available at ScienceDirect

Trends in Analytical Chemistry

journal homepage: www.elsevier.com/locate/trac

A review of calibration-free laser-induced breakdown spectroscopy

Zhenlin Hu [a], Deng Zhang [a], Weiliang Wang [a], Feng Chen [a], Yubin Xu [a], Junfei Nie [a], Yanwu Chu [b, **], Lianbo Guo [a, *]

[a] Wuhan National Laboratory for Optoelectronics (WNLO), Huazhong University of Science and Technology, Wuhan, Hubei, 430074, China
[b] Institute of Optics and Electronics, Chinese Academy of Sciences, Chengdu, Sichuan, 610209, China

Available online 2 April 2022

Keywords:
Calibration-free laser-induced breakdown spectroscopy
Quantitative analysis
Local thermodynamic equilibrium

A B S T R A C T

As an important branch of laser-induced breakdown spectroscopy (LIBS), calibration-free LIBS (CF-LIBS) is a famous element quantitative analysis method without standards. This method has many advantages such as real-time, in-situ, on-site, single-point, and multi-elemental analysis, with excellent potential for geology, archaeology, industrial and environmental monitoring, and biomedicine. In this review, we summarized the development of CF-LIBS. It covered a brief description of the basic theory of CF-LIBS, several modified methods and variants, proposed to overcome the non-stoichiometric ablation, self-absorption effect, and high algorithmic complexity. Furthermore, the applications of CF-LIBS in a variety of fields were reviewed. Finally, the existing problems of CF-LIBS and its potential were discussed.

1. Introduction

Laser-induced breakdown spectroscopy (LIBS) is a well-known elemental analytical technique based on detecting the optical emission from the laser-ablated plasma onto sample surface [1–3]. The spectral signals in the optical emission can determine the element species and concentrations in the sample. With its unique advantages of minimal or no sample preparation, in-situ, rapid, remote, and multi-elemental detection [2,4,5], LIBS has been applied to many fields such as metallurgy [6,7], energy [8–10], mining [11–13], advanced manufacturing [14–17], environmental monitoring [18,19], biomedicine [20–22], single-particle detection [23,24], and space exploration [25–29]. In particular, the Mars explorations by NASA's Perseverance rover and CNSA's Zhurong rover demonstrate the advantages and capabilities of LIBS in extreme environments [30].

For quantitative analysis of LIBS, many calibration strategies have been widely used, including univariate calibration, internal standardization, and standard addition [31,32]. These methods require several standards, containing the gradient target element contents, to build calibration curves. However, LIBS quantitative analysis is dramatically affected by differences in physical and chemical properties between analyzed samples and standards, which is called the matrix effect, both the chemical matrix effect due to the chemical composition of the sample and the physical matrix effect due to the physical state and especially the surface physical properties of the sample [31,33]. The internal standardization can correct the matrix effect by the internal element, but the effect is limited. The standard addition can overcome the matrix effect by adding standards into the aliquots of analyzed samples, only suitable for solution and powder. The multivariate regression methods, including classical chemometric methods, machine learning, and recently developed transfer learning models [34,35], are widely used for LIBS quantitative analysis. These methods can well compensate for the matrix effect but require a large number of standard samples to train the regression model [36,37].

When LIBS is applied in jewellery appraisal [38], geology [39,40], archaeology [41], and biomedicine [42,43], the quantitative analysis via calibration methods often fails because of the lack of matrix-matched standards and high requirements for calibration curves. Several attempts to reduce the number of standards have been reported, including calibration-free LIBS (CF-LIBS) [44], CSigma LIBS (Cσ-LIBS) [45], one-point and multi-line calibration LIBS (OP-MLC-LIBS) [46], single-sample calibration LIBS (SSC-LIBS) [47], etc. The Cσ-LIBS, OP-MLC-LIBS, and SSC-LIBS require one matrix-matched standard, and in comparison, CF-LIBS does not, which was proposed by Ciucci et al., in 1999 [44]. This method can directly use some atomic parameters to calculate the plasma parameters and elemental composition by using the mathematic models of the laser-induced plasma emission, which will be

* Corresponding author.
** Corresponding author.
E-mail addresses: ctguchu@foxmail.com (Y. Chu), lbguo@hust.edu.cn (L. Guo).

https://doi.org/10.1016/j.trac.2022.116618
0165-9936/

described in detail in the next section. Hence, CF-LIBS eliminates the matrix effect by taking the matrix into account as a part of the analytical problem and enables direct quantitative analysis without standards.

Due to the unique advantages, CF-LIBS has excellent potential for real-time, in-situ, online, single-point, and multi-elemental analysis. Nonetheless, several technical challenges exist in CF-LIBS applications due to the strict using conditions and complex algorithms. To give an overview of CF-LIBS and facilitate understanding its theory, we summarized the development of CF-LIBS in this review. It covered a brief description of the basic theory of classical CF-LIBS, several improved CF-LIBS methods, variants, and the calibration-free methods based on other frameworks. Then, the applications of CF-LIBS were briefly reviewed. In the end, existing problems and the outlook were discussed.

2. Basic theory of classical CF-LIBS

2.1. Basic assumptions

When we use CF-LIBS, several basic assumptions should be allowed [48–50]:

I. stoichiometric composition is satisfied; The elemental compositions in sample and plasma are consistent;
II. the plasma is in local thermodynamic equilibrium (LTE); In LTE, excited states are populated according to the Boltzmann distribution, and ionization states are populated according to the Saha-Boltzmann equilibrium equation;
III. the spectral lines are optically thin, which means that the self-absorption effect can be ignored;
IV. the plasma is considered to be spatially homogeneous in the line of sight.

Besides the above assumptions, several experimental requirements also need to be considered: the spectral measurement range of the spectrograph includes measurable spectral lines from all the elements present in the sample. The efficiency of the spectral detection system needs to be measured in advance. The spectral parameters of each spectral line must be known, which are used to determine the plasma temperature through the Boltzmann plot [51] or Saha-Boltzmann plot method [52]. The transition probability, energy, and degeneracy of level are often obtained from the National Institute of Standards and Technology (NIST) atomic spectra database [53] and the atomic spectral line database from CD-ROM 23 of R. L. Kurucz [54]. The Stark parameters can be obtained from the STARK-B database [55] or by bibliographic searching. When the transition probabilities and Stark broadening coefficients are not recorded in databases mentioned above or in literature, LIBS can also be used as a viable measurement tool [56].

However, the ideal laser-induced plasma is hard to obtain in actual experiments. The departure from the basic assumptions often causes unsatisfactory quantitative results, even leads to quantitative failure. Non-stoichiometric ablation is particularly evident in laser ablation analysis for solids, such as LIBS and laser ablation inductively coupled plasma mass spectrometry (LA-ICP-MS) [57]. The self-absorption effect always exists, which is that the plasma emission is re-absorbed by the same kind of ground-state particles when the plasma becomes colder [58,59]. Besides, the LTE assumption is generally considered valid during the detection time window in LIBS [60–62]. In the following sections, the standard procedure of the classical CF-LIBS and several solutions proposed for the failure of basic assumptions will be introduced.

2.2. Classical CF-LIBS based on Boltzmann plot

The standard procedure of classical CF-LIBS based on the Boltzmann plot has been described in detail in many pieces of literature; therefore, here we only give a brief introduction. According to the Boltzmann distribution in an LTE approximation, the integral intensity of the spectral line can be expressed as [44]:

$$I_{ki} = n_s A_{ki} g_k \frac{exp\left(-\frac{E_k}{K_B T}\right)}{U_s(T)} \tag{1}$$

where n_s is the number density (particle/cm^3) of the species s; A_{ki} is the transition probability between the two levels; g_k is the degeneration of the upper level; T is the plasma temperature; E_k is the energy of the upper level; K_B is the Boltzmann constant. The integral intensity I_{ki} is expressed in photon s^{-1}cm^{-3}; $U_s(T)$ is the partition function of the s at plasma temperature T, which can be calculated as:

$$U_s(T) = \sum_j g_j \cdot exp\left(-\frac{E_j}{K_B T}\right) \tag{2}$$

Considered with the efficiency of the spectral detection system, Eq. (1) can be rewritten as:

$$\overline{I_{ki}} = F n_s A_{ki} g_k \frac{exp\left(-\frac{E_k}{K_B T}\right)}{U_s(T)} \tag{3}$$

where $\overline{I_{ki}}$ is the measured integral intensity corrected by the optical efficiency curve; F is an experimental parameter of the efficiency of the spectral detection system as well as the plasma density and volume.

Now we can define the following quantities:

$$y = \ln \frac{\overline{I_{ki}}}{A_{ki} g_k} \tag{4a}$$

$$x = E_k \tag{4b}$$

$$m = -\frac{1}{K_B T} \tag{4c}$$

$$q_s = \ln \frac{F n_s}{U_s(T)} \tag{4d}$$

By rearranging the terms and applying *ln* to both sides to eliminate the exponential function, Eq. (3) can be linearized as:

$$y = mx + q_s \tag{5}$$

The two-dimensional space identified by the above-defined x and y coordinates is called the Boltzmann plane, in which each spectral line is represented as a point. According to Eq. (4c), the plasma electron temperature can be obtained by linear regression of the points representing lines of the same species. According to Eq. (4d), the intercept q_s contains the information of the number density of each species. The experimental parameter F can be obtained by the closed equation:

$$\sum_s n_s = \frac{1}{F} \sum_s U_s(T) \cdot exp(q_s) = 100\% \tag{6}$$

Then, the number density of each species can be calculated by:

$$n_s = \frac{U_s(T)\cdot exp(q_s)}{F} \tag{7}$$

where all the factors are known. Finally, the number density of one target element is the sum of the values corresponding to the neutral and singly ionization states of the same element. The higher ionization states can be ignored due to a small amount of ionization. Once the total number densities of all the elements have been calculated, the relative mass fraction C_a^m of element a can be determined as:

$$C_a^m = \frac{\left(n_a^I + n_a^{II}\right)M_a}{\sum_s n_s M_s} \tag{8}$$

where M_a is the atomic mass of element a. The sum includes all the elements.

2.3. Assisted with Saha-Eggert equation

The Saha-Eggert equation is another numerical relationship obeyed by the particles in LIBS, besides the Boltzmann distribution. When the number of atomic spectral lines is not enough to draw Boltzmann plot, and meanwhile ionic spectral lines of the same element exist, or the opposite, Saha- Eggert equation can be used into CF-LIBS, which describe the populations of the neutral and singly ionization states of the same element as [63]:

$$N_e\frac{n_s^{II}}{n_s^I} = 2\frac{U^{II}(T)}{U^I(T)}\frac{(2\pi m_e K_B T)^{\frac{3}{2}}}{h^3}exp\left(-\frac{E_{ion}}{K_B T}\right) \tag{9}$$

where the indices I and II represent the neutral and singly ionization states of the same element, respectively; m_e is the electron mass; h is the Planck constant; E_{ion} is the first ionization energy; N_e is the electron number density, which is usually calculated by Stark broadening [64].

Replacing n^I and n^{II} in Eq. (9) by intensities of the spectral lines from Eq. (3), the intensity of the ionic line can be rewritten as:

$$I_{jh}^{II} = Fn_s^I A_{jh}^{II} g_j^{II}\frac{\exp\left(-\frac{E_j^{II}}{K_B T}\right)}{U^I(T)}\cdot\left(\frac{2(2\pi m_e K_B T)^{\frac{3}{2}}}{N_e h^3}\right)\cdot exp\left(-\frac{E_{ion}}{K_B T}\right) \tag{10}$$

Rearranging the terms and applying *ln* to both sides, Eqs. (3) and (10) can be expressed as:

$$y^* = m'x^* + q_s' \tag{11}$$

where

$$y^* = \begin{cases} \ln\left(\frac{I_{ki}^I}{A_{ki}^I g_k^I}\right) atomic \\ \ln\left(\frac{I_{jh}^{II}}{A_{jh}^{II} g_j^{II}}\right) - \ln\left(\frac{2(2\pi m_e K_B T)^{\frac{3}{2}}}{N_e h^3}\right) ionic \end{cases} \tag{12a}$$

$$x^* = \begin{cases} E_k^I \; atomic \\ E_j^{II} + E_{ion} ionic \end{cases} \tag{12b}$$

$$m' = -\frac{1}{K_B T} \tag{12c}$$

$$q_s' = \ln\frac{Fn_s^I}{U^I(T)} \tag{12d}$$

The next steps to determine the element concentration are similar to the above [63]. Besides, when only the atomic spectral lines of one element are detected, we can also calculate the concentration of the singly ionization states by the concentration of the neutral atom using Eq. (8), and vice versa [44].

2.4. Evaluation indexes

CF-LIBS is a multi-elemental quantitative method without standards and calibration curves, so the routine statistical analysis of LIBS quantitative results is unsuitable [48]. A simple evaluation index to quantify the difference between certified and predicted contents is necessary. The relative error (RE) is often used to evaluate the quantitative accuracy of CF-LIBS [65–69]. But RE has a flaw due to the normalizing condition described as Eq. (6). The slight REs of major elements will cause large REs of minor elements, even larger than 50% (shown in Table 2). Thus, the mean relative error (MRE) may be unsuitable for the overall accuracy analysis of CF-LIBS, especially in the case that many minor elements exist in the sample.

Because the MRE may not provide a correct evaluation of the CF-LIBS quantitative results, Tognoni et al. [48] proposed a measure named *dist*, which was the Manhattan distance actually. The certified content values and quantitative results of CF-LIBS expressed as percentages can be represented by the vectors C_s and M_s, respectively. The distance between the two vectors is expressed as:

$$dist = \sum_{s=1}^{N}|C_s - M_s| \tag{13}$$

where index s represents various elements, the percentage sign (%) of C_s and M_s is removed. According to Tognoni et al., the accuracy of major elements has a great weight on the *dist*. A *dist* of a few units is a reasonably good result, while a *dist* of the order of tens can be considered as a poor result. The mean absolute error (MAE) was also adopted in some works [70,71], similar mathematically to the *dist*, but easier to understand. When multi-elemental quantitative results of CF-LIBS need to be evaluated comprehensively, we suggest *dist* and MAE as the evaluation indexes, because both of them balance the weights of major and minor elements. If the quantitative targets are major elements, the abovementioned indexes may not be very different, as listed in Table 1.

2.5. Compensating for non-stoichiometric ablation

The main mechanisms during nanosecond pulsed laser ablation for solid samples are heating, melting, sublimation, vaporization, and ionization [73]. Non-stoichiometric ablation occurs before ionization. The element composition of vaporized substances differs from that of the samples due to the difference in heat capacity and enthalpy between different elements [74]. The laser parameters, material properties, and ambient gas also play an essential role in non-stoichiometric ablation. During ionization, the element composition of vaporized substances keeps constant.

Table 1
Evaluation indexes used in CF-LIBS.

Index	Formula	Description	Ref.
RE	$RE = \frac{\lvert C_s - M_s \rvert}{C_s} \times 100\%$	Relative error between certified and predicted content	[65]
MRE	$MRE = \frac{1}{N}\sum_{s=1}^{N}\frac{\lvert C_s - M_s \rvert}{C_s} \times 100\%$	Mean relative error between certified and predicted content	[68]
MAE	$MAE = \frac{1}{N}\sum_{s=1}^{N}\lvert C_s - M_s \rvert$	Mean absolute error between certified and predicted content	[70]
dist	$dist = \sum_{s=1}^{N}\lvert C_s - M_s \rvert$	Manhattan distance between certified and predicted content vectors	[48]
distance	$distance = \sqrt{\sum_{s=1}^{N}\left(\frac{C_s - M_s}{C_s}\right)^2}$	A custom distance between certified and predicted content vectors	[72]

Lednev and Pershin [75] proposed an approach named corrected CF-LIBS (CCF-LIBS) methods to compensate non-stoichiometric ablation, determining the "work function" W_i as:

$$W_i = \begin{pmatrix} c_{i\_solid}\left(T_{i\_melt} - T_{room}\right) + \Delta H_{i\_fusion} \\ +c_{i\_liquid}\left(T_{i\_evap} - T_{i\_melt}\right) + \Delta H_{i\_evap} \end{pmatrix} T_{i\_melt} \quad (14)$$

where i represents one element; c_{i_solid} is the heat capacity of the solid; c_{i_liquid} is the heat capacity of the liquid; T_{room} is room temperature; T_{i_melt} is the melting temperature; T_{i_evap} is the temperature of the evaporation; ΔH_{i_fusion} is the enthalpy of the melting; ΔH_{i_evap} is the enthalpy of the evaporation. The "work function" depending on the thermal parameters of the target components can correct the biased spectral intensity by:

$$\overline{I_{ki}} = F\frac{C_s}{M_s W_i}A_{ki}g_k\frac{exp\left(-\frac{E_k}{K_B T}\right)}{U_s(T)} \quad (15)$$

The authors calculated the concentrations of Li, Mg, and Al in alloys by CCF-LIBS and classical CF-LIBS, respectively. Compared

Table 2
Quantitative accuracy of various CF-LIBS methods.

Year	Methods	One certain sample	Quantitative results				Ref.
			Major elements[a]	REs (%)	Minor or trace elements[b]	REs (%)	
1999	CF-LIBS based on Boltzmann plot	Aluminum alloy	Al[d], Si	0.36, 38	Mg, Fe, Mn, Cr, Zn, etc.	2.22–30	[44]
2002	CF-LIBS with self-absorption correction by COG	Steel	Mn, Ni, Cr, Mo, Fe[d]	16.5, 10.5, 3.52, 42.9, 0.84	/	/	[77]
2006	CF-LIBS based on synthetic spectra	Bauxit	Al, Fe, Si, Ti	25–30	/	/	[89]
2007	CF-LIBS based on Saha-Boltzmann plot	Aluminum alloy	Al[d], Mn	1.02, 39.8	Fe, Mg, Cu	10, 13.5, 72.7	[63]
2007	SC-LIBS	Bronze	Sn, Pb	12.2, 64.4	Ni	45.6	[80]
2008	CF-LIBS with non-stoichiometric ablation correction	Aluminum alloy	Li, Mg, Al[d]	10, 21.5, 0.59	/	/	[75]
2009	CF-LIBS with IRSAC	Aluminum alloy	Cu, Al[d]	20.1, 0.51	Mn	42	[65]
2012	Inverse CF-LIBS	Brooch	Sn	2.69	Pb, Zn, Ag	16.3, 18.2, 83.3	[81]
2013	OPC-LIBS based on Boltzmann plot	Bronze	Cu[d], Zn, Sn, Pb	1.19, 0, 0.95, 31.3	/	/	[82]
2015	CF-LIBS with IRESIC	Bronze	Al, Cu[d], Fe, Mn	5.24, 0.05, 2.08, 21.1	/	/	[67]
2016	Electron number density conservation method	Pb–Sn alloy	Pb[d], Sn	1.86, 2.47	/	/	[93]
2017	CF-LIBS with standard reference line[c]	Steel	Cr, Fe[d], Si	dist <10[c]	Al, Mn, Ni	/	[84]
2019	CF-LIBS with BRR-SAC	Titanium alloy	Ti[d], V, Al	0.47, 4.42, 3.85	/	/	[70]
2019	OPC-LIBS assisted with Saha-Boltzmann plot	Pellet (CaCO3, TiO2, CuSO4, NaCl)	C	<10	/	/	[83]
2021	CF-LIBS with CD-SRL	Bronze	Cu[d], Al, Fe, Mn	1.17, 11.6, 19.6, 35	/	/	[71]

[a] Concentrations range from 1 wt% to 100 wt%.
[b] Concentrations are less than 1 wt%.
[c] Only the dist [48] of quantitative results of all elements was given in the paper.
[d] The matrix element, whose concentration is more than 50 wt%.

with classical CF-LIBS, the RE of CCF-LIBS was reduced dramatically for three elements.

Matsumoto et al. [76] estimated the Zn/Cu ratio in an aqueous solution using electrodeposition-assisted underwater CF-LIBS. They corrected the calculation deviation of the Zn/Cu ratio between in the deposit and in the plasma using a simple model considering heat propagation and thermal evaporation during liquid-phase laser ablation.

In recent years, most researchers usually did not consider the non-stoichiometric ablation in CF-LIBS. But when the predicted content by CF-LIBS is far from certified one, it may be a possible reason.

2.6. Compensating for self-absorption effect

Self-absorption is a common phenomenon in LIBS. The line with lower energy upper level or a higher transition probability is affected by the self-absorption more severely, causing a nonlinearity in the Boltzmann plot [65]. Thus, the calculated value of the plasma electron temperature and concentrations will deviate from the actual one. The self-absorption correction is restoring the affected spectral intensity, and lots of self-absorption correction methods have been proposed [59]. Here, we only introduce three typical correction approaches for CF-LIBS.

To correct self-absorption in CF-LIBS, Bulajic et al. [77] proposed an automatic correction procedure using the curve of growth (COG) method [78,79]. The input parameters of this procedure were the plasma electron temperature, the electron density, the Lorentzian and Gaussian half-widths, and the optical path length. Then, the experimental line intensities should be corrected by an iterative algorithm. The authors applied this procedure in three-ternary alloys of Au, Ag, and Cu, and three steel NIST standards, which showed better quantitative results than those without correction. However, the calculation process of this method is quite complicated.

Sun and Yu [65] proposed a simplified procedure named internal reference for self-absorption correction (IRSAC) in CF-LIBS. For each species, the authors selected a spectral line with a high upper energy level or low transition probability as the internal reference line whose self-absorption was negligible. Then, they evaluated the self-absorption extent of other lines by the intensity of the internal reference line and corrected the affected line intensities by a recursive algorithm. The authors tested this procedure on the aluminium alloy and the iron-chromium-nickel alloy samples, gaining more accurate quantitative results than before. After IRSAC, the fitting lines of each species in the Boltzmann plot became parallel, as shown in Fig. 1. The simplicity of this method is that only a spectral line without self-absorption is needed. It should be noted that the reference line selection must be careful, considering the accuracy of transition probability and the signal-to-noise ratio.

Dong et al. [67] proposed an internal reference-external standard with iteration correction (IRESIC) method to correct the self-absorption effect and plasma temperature in CF-LIBS based on an internal reference line and one standard sample. This improved method corrected spectral line intensities by IRSAC and used one standard sample with the genetic algorithm (GA) to determine the plasma temperature of the unknown samples. Yang et al. [68] improved the IRSAC method by developing an automatic internal reference line selection program and estimating the plasma temperature by the particle swarm optimization (PSO) algorithm.

Li et al. [70] proposed a self-absorption correction method named blackbody radiation referenced self-absorption correction (BRR-SAC). The authors used an iterative method to calculate the plasma temperature and the efficiency of the optical collection system by comparing the measured spectrum and blackbody radiation intensity. The experimental results illustrated that the quantitative errors of the titanium alloy sample with BRR-SAC were even smaller than those with IRSAC. Fig. 2 showed the spectrum of the titanium alloy sample before and after BRR-SAC. According to the authors, this method is quite suitable for the sample with many spectral lines, such as steel and titanium alloy.

3. Improved CF-LIBS methods and variants

In practice, there are still quantities of problems to perform the standard procedure of classical CF-LIBS mentioned in Section 2. The accuracy of classical CF-LIBS depends on the choice of suitable spectral lines and the accurate fitting of straight lines in the Boltzmann or Saha-Boltzmann plane. The accurate fitting leads to the accurate estimation of the plasma temperature and element content. However, not all elements have enough spectral lines to draw the Boltzmann or Saha-Boltzmann plot. Even if the number of lines is enough, not all their atomic parameters recorded in databases are precise. Besides, the quantitative results of trace elements only reach a semi-quantitative level. Sometimes, measuring the efficiency of optical systems is a challenge. The following section introduces several improved methods and variants of classical CF-LIBS aiming to overcome these problems. Then some calibration-free approaches based on other theoretical frameworks are also introduced.

3.1. Self-calibrated LIBS (SC-LIBS)

Self-calibrated LIBS (SC-LIBS) was proposed by Giacomo et al. [80] in 2007. This method used the optical system efficiency to link

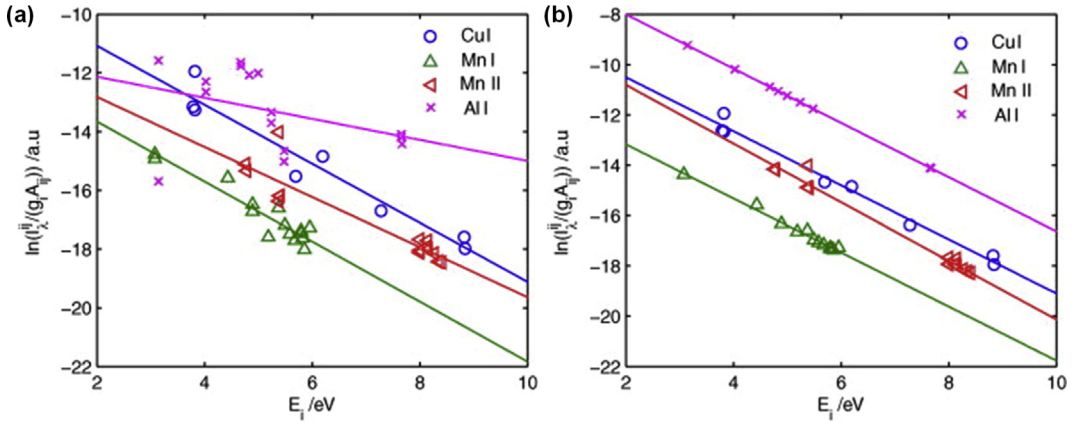

Fig. 1. a) The Boltzmann plot of the aluminum alloy sample before, and b) after self-absorption correction by IRSAC [65].

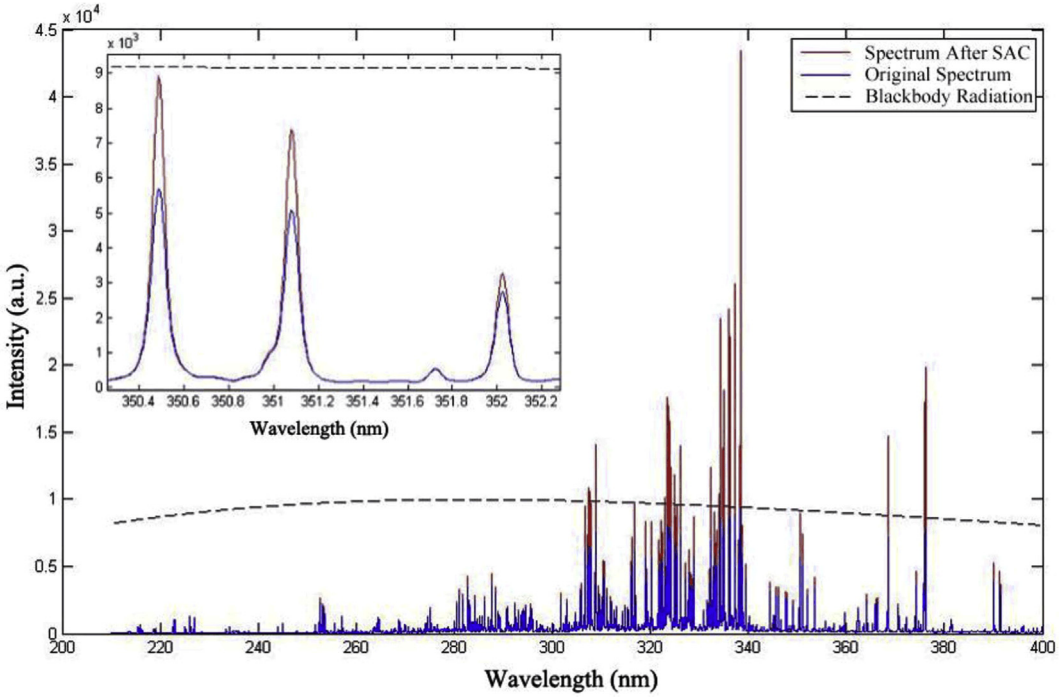

Fig. 2. The spectrum of the titanium alloy sample before and after BRR-SAC together with blackbody radiation [70].

the continuum background radiation in the early stage of plasma evolution to line emission in the later stage, described as:

$$ln\left(\frac{I'_{ul}}{I'_{bkg}}\right) = ln\frac{n_s}{U(T_{exc})} - \left(\frac{E_k}{K_B T_{exc}} - \frac{hc}{T_{bkg}}\right) \tag{16}$$

where I'_{ul} is the line emission intensity; I'_{bkg} is the continuum background intensity assumed to follow a Planck-like distribution; T_{exc} is the excitation temperature in the later stage; T_{bkg} is the temperature of blackbody emission in the early stage; c is the velocity of light.

The plasma temperature can be calculated using the continuum background and line emission intensities without calculating the optical system efficiency in advance. After the plasma temperature is estimated, the number density of each species can be calculated directly by only one spectral line. It should be noted that plasma fluctuations may greatly reduce the accuracy of this method unless two spectrometers are available to measure the spectrum of the same plasma in the different stages. Multiple acquisitions and averaging of spectra could be also a solution.

3.2. Calibration-free inverse method

Gaudiuso et al. [81] suggested the calibration-free inverse method in 2012. This method could determine the optimum plasma temperature by minimizing the absolute difference between the nominal and calculated composition of the standard as:

$$\Delta(T) = \sum_i \frac{\left|w\%^i_{cert} - w\%^i_{CF}(T)\right|}{w\%^i_{cert}} \tag{17}$$

where $w\%^i_{cert}$ and $w\%^i_{CF}(T)$ are the certified content of the element i and content of the element i calculated by CF-LIBS at the plasma temperature T, respectively. Then the authors used the calculated optimum plasma temperature to quantify the unknown samples in the framework of the classical CF-LIBS.

3.3. One point calibration LIBS (OPC-LIBS)

To improve the reliability of the CF-LIBS analysis, Cavalcanti et al. [82] proposed the one-point calibration LIBS (OPC-LIBS) in 2013. The main idea of this method is that the best values of the $P(\lambda) = F(\lambda)A_{ki}g_i$ can be empirically determined using the Boltzmann plot of the known sample. Then the $P(\lambda)$ values can be used to quantify unknown samples by CF-LIBS. Because $F(\lambda)$, A_{ki}, and g_i are determined as a whole by the known sample, OPC-LIBS can overcome the inaccuracy of transition probability A_{ki} and the difficulty of measuring the efficiency of the optical system. Fig. 3 illustrates how this method works.

Borduchi et al. [83] improved the OPC method assisted with the Saha-Boltzmann plot, which was used to obtain the more precise evaluation of the plasma temperature and electron density. The authors tested this modified OPC-LIBS on two sample sets with different C concentrations, which contained graphite and calcium carbonate in a matrix of sodium chloride, respectively. Compared with the OPC method only applied to the Boltzmann plot, the uncertainty of the plasma temperature and electron number density reduced from 2.3% to 0.5%, obtained by the Saha-Boltzmann plot with the OPC. Using the OPC method assisted with the Saha-Boltzmann plot also provided more precise quantitative results than the OPC method with the Boltzmann plot. The uncertainties of the estimated C concentration were decreased significantly.

3.4. CF-LIBS with the standard reference line

In the Boltzmann plot, the fitting straight line for each element requires at least two points, calculated from two spectral lines with different upper energy levels. The line number of the trace element is often hard to meet this requirement. In 2017, the CF-LIBS with the standard reference line (SRL) method, proposed by Fu et al. [84], overcame this disadvantage. The author used the matrix element to

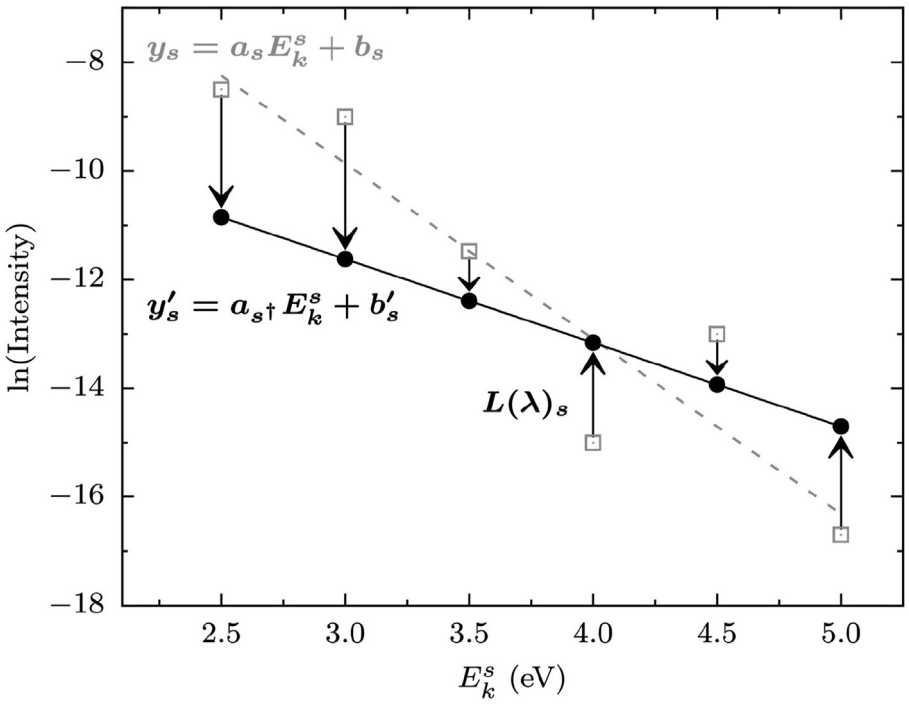

Fig. 3. OPC correction of a Boltzmann plot of species *s*. Open grey squares correspond to uncorrected points, while the black-filled circles are points corrected by the OPC method. Straight lines are linear fit of uncorrected (grey dashed line) and corrected points (solid black line) [82].

determine the plasma temperature by the Saha-Boltzmann plot. When the plasma temperature was known, all the element concentrations could be calculated by Eqs. (3), (4d), 6 and 8 using one reference line chosen for each element. The authors tested the proposed method in the stainless steel sample. Firstly, they precisely calculated the plasma temperature using the rich lines of Fe and the electron density by the Stark broadening of Fe I 381.584 nm. Although Fe is the matrix element, the optically thin lines of Fe are enough to draw the Boltzmann plot. Then, they selected one optically thin line for each element to deduce the number density. This method has no requirement for the line number of minor and trace elements, dramatically improves the operability of CF-LIBS, and shortens the calculation times. They also combined the SRL method with OPC to further increase the quantitative accuracy [85], but the difference in the sum of absolute errors is not obvious between the SRL method with OPC and the original SRL method.

3.5. Combination with machine learning

D'Andrea et al. [86] proposed an artificial neural network (ANN) quantitative model without standards, where the ANN is trained using the simulated LIBS spectra. Its inputs were line intensities of the simulated spectra, and output was the Ni concentration of the samples. However, the prediction precision of this simple ANN is poor. Thus, they proposed a “hybrid” ANN approach. The ANN is trained using the simulated spectra and the CF-LIBS calculation of the electron temperature and electron number densities. Its outputs were the values of the Ni concentration, plasma temperature, and electron number density. According to the authors, this ANN model could achieve a precise quantitative analysis even in relatively large laser fluctuations and matrix effects.

3.6. Other theoretical frameworks

Determining elemental concentrations by matching experimental and synthetic LIBS spectra is another common calibration-free approach. This method was firstly used by Gornushkin et al., in 2004, named Monte-Carlo LIBS (MC-LIBS) [87,88]. They used the model of the post-breakdown LTE plasma to produce synthetic LIBS spectra. The plasma temperature and number densities of species were taken as model input parameters. Then the search for the best fit between experimental and synthetic spectra was performed using a Monte Carlo approach to minimize multivariate functions. The high quantitative accuracy was based on several hours of computation, which limited the application of MC-LIBS. Yaroshchyk et al. [89] suggested an easier LTE model, taking plasma temperature and electron density into account as well as the characteristics of atomic emission transitions as main input parameters. Compared with Gornushkin's model, the time complexity was significantly reduced. Demidov and Gornushkin et al. [90] used graphic processing unit (GPU) computation to reduce the analysis time of MC-LIBS down to several seconds per spectrum/sample. They tested the improved GPU-based MC-LIBS on the stimulated steel slag with the RE between 1% and 10%. D'Andrea et al. [86] used the synthetic spectra to train the ANN regression model, which was not precise. Kumar et al. [91] improved the method proposed by Yaroshchyk, considering the self-absorption effect of spectral lines. Compared with previous works [88,89], Kumar's method could simulate a more extended spectra range and obtain higher quantitative accuracy. MC-LIBS is time-consuming but promising as the further improvement of the plasma theory in LIBS.

The optical depth method was proposed by Cristoforetti and Tognoni [92] in 2013. This method could estimate the concentration ratios between self-absorbed elements via the columnar density and Saha-Boltzmann distribution. The authors suggested a new approach, named Columnar Density Saha-Boltzmann (CD-SB) plot to calculate the plasma temperature. After the plasma temperature was estimated using the CD-SB plot, the calibration-free quantitative analysis of self-absorbed elements could be performed by columnar density calculated by optical depth. Optical depth could be calculated by line width and self-absorption coefficient *SA*. Our Group proposed a hybrid CF-LIBS approach, named

CF-LIBS with columnar density and standard reference line (CF-LIBS with CD-SRL) [71]. We combined the optical depth method and CF-LIBS with the standard reference line (SRL), extending to self-absorbed and less self-absorbed elements. After determining the plasma temperature by the CD-SB plot, CF-LIBS with CD-SRL could calculate the content ratios between major elements by columnar density. Then we could use the SRL method to calculate the content ratios of one major element to each minor element. Finally, all elements' contents could be calculated using the content ratios between all the major elements and one major element to each minor element. This method has good operability in the case that most lines of major elements are self-absorbed, and lines of minor and trace elements are lacking. The accuracy of this method also depends on the chosen reference line like all the CF methods combined with the SRL method.

Abbass et al. [93] suggested the electron number density conservation method. This method was based on that the total electron number density N_e was the sum of the electrons from all the elements. The authors estimated the plasma temperature and electron number density by the Boltzmann plot and Saha-Boltzmann equation, respectively. By comparing the supposed and calculated values of N_e, the number densities of elements in the plasma could be calculated iteratively. They performed the proposed method on Pb—Sn alloys and obtain better quantitative results than classical CF-LIBS. In contrast to classical CF-LIBS, this method did not require drawing the Boltzmann plots for all the elements present in the sample but depended on the precise measurement of N_e.

4. Applications of CF-LIBS

Since CF-LIBS was proposed in 1999, it has been preliminarily applied in many fields, such as metallurgy, geology, archaeology, biomedicine, materials science, and environment monitoring. The reason for CF-LIBS being chosen in these fields is often because of the lack of standards and the need for in-situ analysis. Fig. 4 shows the number of publications of CF-LIBS for 23 years with an overall upward trend. Data were obtained from Web of Science. In this section, we focus on several representative application fields of CF-LIBS. Typical applications of CF-LIBS are presented in Table 3, together with the target elements, instrument type, and experimental parameters.

4.1. Metallurgy

The metallurgical industry is one of the basic industries of a country and plays an essential role in strengthening the economy. In the metallurgical industry, it is necessary to monitor the elemental content of intermediates and carry out rapid, in-situ elemental analysis of finished products. The routine analytical techniques, such as atomic absorption spectrometry (AAS), energy dispersive X-ray spectrometry (EDX), and inductively coupled plasma mass spectrometry/optical emission spectrometry (ICP-MS/OES), need to transfer samples to the laboratory and complex sample preparation, which is time-consuming and off-line. X-ray fluorescence (XRF) might cause radiation exposure and a high limit of detection (LOD). Because LTE is easy to be satisfied in alloys [61,62], CF-LIBS is especially suitable for the non-standard detection of solid and molten alloys.

Aguilera et al. [72] carried out CF-LIBS on the spatially resolved spectra of a Cu-based alloy acquired by an imaging spectrometer coupled to an intensified CCD (ICCD), taking a 1064 nm Nd: YAG laser as the excitation source. The experimental results illustrated that the quantitative accuracy of the central region of the plasma is higher than the spatially integrated spectrum. Sun et al. [66] tested CF-LIBS on wrought aluminium alloy samples using a 532 nm Nd: YAG laser and a 4-channel fiber-optic spectrograph. Al, Cu, Mg, Mn, Fe, Si, and Zn present in samples were quantified with maximum and minimum relative errors (REs) of 18.4% and 0.36%, respectively. Shah et al. [94] used a 532 nm Nd: YAG laser and an echelle spectrometer with ICCD to quantify Fe, Cr, Mn, and Si in steel samples by CF-LIBS with REs less than 5%. Kolmhofer et al. [95] analyzed the principal oxides in steel slag by CF-LIBS. The CF-LIBS results of CaO, Al_2O_3, MgO, SiO_2, and MnO were similar to those of XRF, but deviations of FeO and TiO_2 were large. Zhu et al. [96] quantified the concentration of elements in molten AZ31 magnesium alloy after long-pulsed Nd: YAG laser processing using CF-LIBS. The results

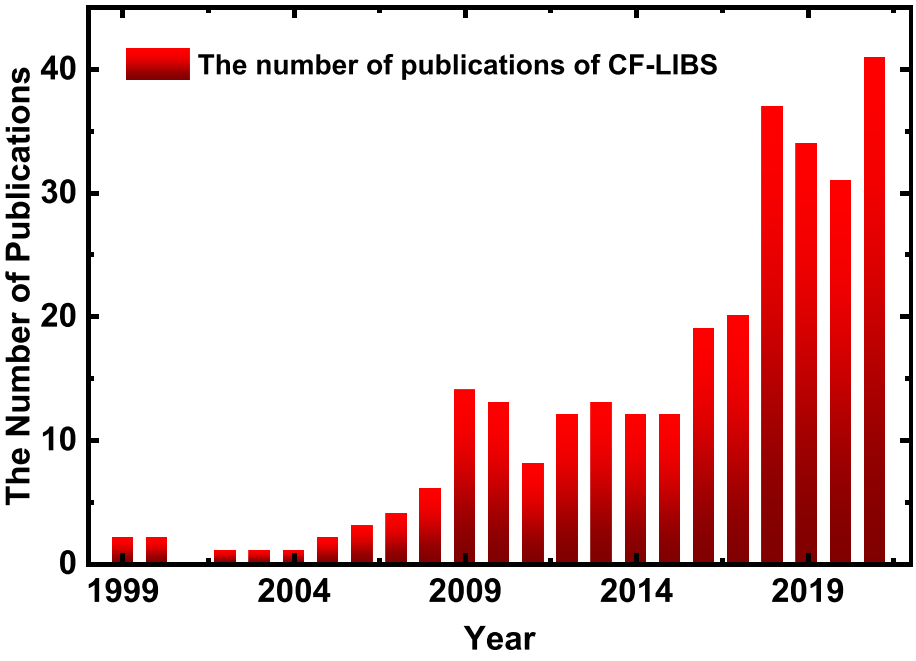

Fig. 4. The number of publications in the Web of Science search by calibration-free laser-induced breakdown spectroscopy (CF-LIBS) in 1999—2021.

Table 3
Typical applications of CF-LIBS.

Sample		Detecting target	Laser			Spectrometer type	Detector type	Ref.
Type	Name		Type	Wavelength (nm)	Pulse duration			
Metallurgy	Copper-based alloy	Cu, Fe, Mn, Ni	Nd: YAG	1064	4.5 ns	Czerny-Turner imaging	ICCD	[72]
	Aluminium alloy	Al, Cu, Mg, Mn, Fe, Si, Zn	Nd: YAG	532	8 ns	Multi-channel fiber-optic	CCD	[66]
	Steel	Fe. Cr. Ni. Mn, Si	Nd: YAG	532	7 ns	Echelle	ICCD	[94]
	Steel slag	CaO, Al_2O_3, MgO, SiO_2, MnO, etc.	Nd: YAG	1064	6 ns	Echelle	ICCD	[95]
	Titanium alloy	Ti, Al, V	Nd: YAG	1064	5 ns	Echelle	ICCD	[69]
Mineral	Volcanic rock	Fe, Si, Mg, Ca, Ti, Mn, Al, Na, etc.	Nd: YAG	355	8 ns	Czerny-Turner imaging	ICCD	[99]
	Ferromanganese nodules	Mn/Fe	Nd: YAG	532	6 ns	Czerny-Turner imaging	ICCD	[105]
	Steatite	Si, Mg, Ca	Nd: YAG	1064	9 ns	Multi-channel fiber-optic	CCD	[104]
Heritage	Mineral pigment	Al/Cu, Na/Cu	Nd: YAG	1064	8 ns	Echelle	ICCD	[110]
	Ancient copper artefact	Ag, Al, As, Ca, Fe, Mg, Na, Pb, Sb, Si	Nd: YAG	1064	8 ns	Echelle	ICCD	[111]
	stone monument	Ca, C, Mg, K, Na, Al, Fe, Si	DPSSL[a]	1064	500 ps	Multi-channel fiber-optic	CCD	[112]
Organism	Coral skeleton	Ca, Sr, Mg, C, O, Na, K, Fe	Nd: YAG	532	4 ns	Multi-channel fiber-optic	CCD	[114]
	Deer bone	Ca, Mg, Sr, Ba	Nd: YAG	1064	5 ns	Echelle	ICCD	[117]
	Human hair & nail	Ca/Na, Mg/Na	Nd: YAG	532	8 ns	Multi-channel fiber-optic	CMOS	[119]
Material	Nanoalloy & nanocomposite	Pt/Ni Pt/Co Co/Pd	Nd: YAG	1064	8 ns	Czerny-Turner imaging	ICCD	[123]
	Nickel-chromium-molybdenum alloy film	Ni, Cr, Mo, Fe, Al, Nb, Si, Co, etc.	Nd: YAG	266	4 ns	Echelle	ICCD	[127]
	Solar cell	Al, C, Ca, Fe, In, Ti, Sb, Sn	Nd: YAG	1064	6 ns	Multi-channel fiber-optic	CCD	[129]
Environmental	Industrial smoke	Al, Ca, Cr, Cu, Fe, Mg, Mn, Na, etc.	Nd: YAG	1064	7 ns	Echelle	ICCD	[131]
	Sludge	Cr, Pb	Nd: YAG	532	4 ns	Multi-channel fiber-optic	CCD	[133]
	Aerosol	Al, O	Nd: YAG	1064	5 ns	Echelle	ICCD	[134]

[a] The diode-pumped solid-state laser (DPSSL).

illustrated that CF-LIBS could obtain satisfactory quantitative or semi-quantitative results for matrix or major elements, while only qualitative results for minor and trace elements. Shakeel et al. [97] quantified Mg, Al, Si, Ti, Mn, etc., in Al–Si alloy with the maximum RE of 6.7%. After IRSAC, the maximum RE was reduced to 2.2%. Hai et al. [69] used OPC-LIBS to determine major and minor elements in titanium alloys. The results were superior to those obtained by the conventional calibration curve and classical CF-LIBS. Urbina et al. [98] proposed a novel CF-LIBS procedure based on the 3D Boltzmann plot to quantify binary alloys. They tested this method on binary Pb–Sn alloys, with REs less than 5%.

4.2. Geology

Geology is not only important for the understanding of Earth's structure, hydrology, and climates but also mineral and hydrocarbon exploration and exploitation. It is also one of the mature application fields of LIBS. In addition to many unique advantages, LIBS development in geology also benefited from Mars exploration. For the chemical analysis of geological materials, the production of standards is always an issue. Meanwhile, the matrix effect impedes the quantitative analysis based on calibration methods, making in-situ analysis of solid samples difficult. CF-LIBS is a feasible solution to this problem, which can realize the quantification of major elements and also reach the level of semi-quantitative analysis for minor and trace elements without standards.

Colao et al. [99] conducted CF-LiBS on 11 elements, including Fe, Si, Mg, Ca, Ti, etc., in 6 earth volcanic rocks similar to the Martian rocks in the simulated Martian environment. The quantitative results were consistent with EDX analysis, with quantitative accuracy ranging from a few percent up to 20–30%. Senesi et al. [100] used the double pulse micro-LIBS system to quantify Ca, Co, Fe, Ga, Li, and Ni in petrographic thin sections of Agoudal iron meteorite. The results were in good agreement with those obtained by traditional methods such as ICP-MS and SEM-EDX. Dell'Aglio et al. [101] used stand-off LIBS to detect two famous meteorites, Toluca (iron meteorite) and Sahara 98,222 (L6 chondrite), at a distance of 5 m and performed calibration-free analysis. This experiment demonstrated the possibility of remote CF-LIBS analysis of minor bodies and space debris. Fahad et al. performed CF-LIBS analysis on quartz-bearing limestone, high silica bauxite, and raw steatite [102–104]. They also adopted other techniques to cross-validate the CF-LIBS results, such as XRF, EDX, X-ray diffraction (XRD), Fourier transform infrared spectroscopy (FTIR). Up to now, CF-LIBS has become a popular in-situ element quantitative method, suitable for various types of geology samples, such as ferromanganese nodules [105], chalcopyrite [106], malachite [107], and Antarctic soils [108].

4.3. Archaeology

The main purpose of archaeology is to learn more about past societies and the development of human beings. It has political and cultural significance, besides scientific importance. After being discovered, excavated, or collected, artifacts need to be dated and their compositions examined comprehensively by many analytical techniques. As an in-situ, on-site, depth-resolved, and multi-element simultaneous quantification technique, CF-LIBS is

particularly suitable in the archaeology field. It can complete the quantitative analysis of various elements through the invisible crater and minimal ablation amount.

Borgia et al. [109] firstly applied CF-LIBS to quantitative analysis of cultural relics. Eleven elements, including Fe, Ca, Ti, Al, Si, etc., present in ancient Roman fresco samples were quantified, and the minimum LOD reached 1 ppm. Bicchieri et al. [110] combined μ-LIBS and the CF procedure to determine the Al/Cu and Na/Cu weight ratios in azurite and lazurite-based pigments. It verified that CF-LIBS was a feasible method for the identification of pigment types on ancient illuminated manuscripts. Corsi et al. [111] determined As, Ag, Al, As, Ca, Fe, etc., in 13 ancient Italian copper artifacts, helping identify the place of origin. Senesi et al. [112] used a handheld LIBS instrument to analyze stone monuments. They determined Ca, C, Mg, K, Na, etc., in stone monuments, which showed handheld LIBS a significant potential in in-situ measurements on outdoor archaeological sites.

4.4. Biomedicine

Living organisms require varying amounts of metallic and nonmetallic elements, such as K, Na, Mg, Ca, Cl, and P, which have vital roles in regulating membrane activity and osmotic potential. Other trace heavy metal elements play a role in determining protein structure. Thus, the elemental analysis of biological tissues is quite significant for the study of life activities. Biological tissue samples are usually heterogeneous and multifarious, whose certified reference material (CRM) is often unavailable. Their sample preparation for common quantification techniques is complex, time-consuming, and hazardous, such as acid, high pressure, or microwave digestion. CF-LIBS is a potential option for elemental quantification and distribution imaging of biological tissues.

Corsi et al. [113] firstly applied CF-LIBS on biological tissues. They determined the main mineral elements present in human hair, which showed the possibility for the fast and inexpensive determination of heavy-metal poisoning in hair using CF-LIBS. Pandhija and Rai [114] used CF-LIBS to determine Ca, Sr, Mg, C, O, Na, K, and Fe in coral samples. The authors found that the results of CF-LIBS were not in agreement with those of ICP-MS. It may be because CF-LIBS analyzes the coral surface, whereas ICP-MS relates to its whole mass. Singh et al. [115] used CF-LIBS to quantify metal elements in three kinds of gallstones and obtained the variation of constituents from the center to the surface of gallstones, which benefited the clinical detection. Iqbal et al. [116] determined the major and minor elements in sage (herb) by CF-LIBS. Roldán et al. [117] quantified the inorganic elements, including Ca, Mg, Sr, and Ba, in deer bone samples by CF-LIBS. Al-Salihi et al. [118] tested CF-LIBS to quantify Mg, Fe, Ca, Na, and K in neoplastic tissues, the results in good agreement with those of ICP-OES. Our group applied CF-LIBS to determine the Ca/Na and Mg/Na weight ratios in human hair and nails. The results showed that the REs between quantitative results of CF-LIBS and ICP-OES were less than 10% [119].

4.5. Material science

Material characterization technique is of great importance for the evaluation of material properties. Compared to energy/wavelength dispersive X-ray spectrometry (EDX/WDX) and XRF, LIBS has the disadvantage of microdamage. However, LIBS does not need samples to be polished and placed in a vacuum. When CF-LIBS is used, the type, state of matter, shape, and size of samples are also unlimited. It can detect most elements on the periodic (from H to Am) table simultaneously and quickly. Due to the advantages mentioned above, CF-LIBS is gradually applied to the elemental characterization of various materials.

Burakov et al. [120] quantified SiO_2, PbO, K_2O, and BaO in glass using CF-LIBS with REs between 0.33% and 39.8%. Praher et al. [121] used CF-LIBS with self-absorption correction to analyze pills containing three kinds of oxide powder, Fe_2O_3, MgO, and CaO. The REs for the three oxides are less than 10%, 20%, and 5%, respectively. Pedarnig et al. [122] quantified oxides in ceramic slag and bulk slag pieces from secondary metallurgy. The former was produced by hydraulic pressing of thoroughly ball milled powder and sintering, and the latter was sampled with an automated system. The results showed that REs decreased with increasing oxide concentration, and LOD was about 1 wt%. Matsumoto et al. [76] used CF-LIBS assisted with electrodeposition to determine the Zn^{2+}/Cu^{2+} weight ratio in an aqueous solution. Davari et al. [123] determined weight ratios of Pt/Ni, Pt/Co, and Co/Pd in intermetallic nanoalloys (NAs) and nanocomposites (NCs) by CF-LIBS, and the results were consistent with those by ICP-OES. They also tested CF-LIBS on quantitative analysis of O/Si ratio in SiO_2 films to identify films of different thicknesses [124]. Pagnotta et al. [125] combined micro-LIBS (μ-LIBS) mapping technique with CF-LIBS so they could quickly obtain quantitative elemental 2D mappings of inhomogeneous samples. Hermann et al. performed the calibration-free quantitative algorithm based on synthetic LIBS spectra on glass, alloy, and thin films [126,127]. Farooq et al. [128] applied CF-LIBS with IRSAC to quantitatively analyze doped nanomaterial containing Fe and Sn nanoparticles. The results by CF-LIBS provided good agreement with data by laser ablation time of flight (LA-TOF) spectroscopy and a slight deviation from EDX. Shakeel et al. [129] used a double-pulse LIBS system and calibration-free method to analyze unknown polycrystalline silicon solar cells containing Al, C, Ca, Fe, In, Ti, Sb, and Sn in the parts per million (ppm). Gerhard et al. [130] adopted the sensitivity-improved CF-LIBS for quantitative analysis of manufacturing-induced trace contaminants of optical glass surfaces. They determined major and minor elements using early measured spectra performed in full LTE and determined trace elements using spectra with larger delay. The authors also performed depth-resolved CF-LIBS and the results were validated by ICP-OES, which determined the bulk glass. In a word, the works mentioned above preliminarily confirmed CF-LIBS as a valid and potential in-situ quantitative technique for various materials.

4.6. Environment monitoring

Environmental pollution seriously endangers the ecological balance and human health. Environmental monitoring can effectively mitigate the risks of environmental pollution. LIBS has many strengths in environmental monitoring, such as remote, in situ, and fast detection, which other element analysis techniques do not. Because CF-LIBS avoids sample preparation and calibration curve, any state and type of samples can be directly quantified by CF-LIBS in various environments.

Corsi et al. [131] applied CF-LIBS to quantify the 16 metal elements, including Al, Ca, Cr, Cu, Fe, etc., in industrial smoke with the LODs of 1 ppm or smaller and precision of 1%. They also compared the single pulse and double pulse CF-LIBS for elemental analysis of the contaminated soil [132]. The experimental results illustrated that double pulse CF-LIBS could detect 8 metal elements while single pulse CF-LIBS could only detect 5 elements. Kumar et al. [133] used CF-LIBS to quantify Cr, Pb, and other harmful elements in industrial sludge and also used the basic calibration method. The results of the two methods were in good agreement, making it possible for CF-LIBS to be used for early warning of heavy metal

pollution in water sources. Boudhib et al. [134] used CF-LIBS based on the synthetic spectra to determine Al and O in Al_2O_3 aerosols. The results showed that the accurate composition determination of aerosol required the spectral acquisition delay to be less than 1 μs when the electron number density was large enough to maintain the Boltzmann equilibrium. Akhtar et al. [135] used magnetic field assisted CF-LIBS and LA-TOF-MS to quantify soil collected from the vicinity of the leather industries. The deviations in the compositional analysis using CF-LIBS and LA-TOF-MS were less than 10%.

5. Conclusions and perspectives

CF-LIBS has been applied as a fast elemental quantitative technique in many fields, especially in geology, archaeology, and biomedicine, since it was first reported in 1999. Quantities of CF-LIBS related works have demonstrated its great potential for in-situ, on-site, online, and multi-elemental microanalysis. In this review, we summarized the basic theory and the developments of CF-LIBS. The basic assumptions and the main algorithm of the classical CF-LIBS were briefly described in Section 2. Several improved CF-LIBS models, variants, and calibration-free methods based on other frameworks were introduced in Section 3. These calibration-free models further improved the quantitative accuracy and broadened the application of CF-LIBS. Finally, the typical applications of CF-LIBS in metallurgy, material science, geology, archaeology, biomedicine, and environment monitoring were briefly recalled in Section 4.

Nevertheless, many problems still exist to hinder the practical applications of CF-LIBS. Firstly, CF-LIBS can only do the semi-quantitative analysis of minor and trace elements, which is an inherent defect of CF-LIBS theory. The reasons include the normalization relationship of elemental contents used in CF algorithm and the nonuniform distribution of minor and trace elements inside the sample or plasma. Secondly, CF-LIBS is still in the theoretical research stage, lacking systematic research on experimental configuration and parameters and the influence of sample characteristics. Thirdly, a set of complete evaluation indexes for CF-LIBS quantitative results is lacking. It should be noted that the spectral data preprocessing and high requirements for instruments are also challenges for practical applications.

Besides, several interesting research areas of CF-LIBS show significant promise. According to the reported works [129,132,136,137], the double-pulse CF-LIBS and ultrafast laser CF-LIBS have higher quantitative accuracy and lower LOD than the single-pulse system. These experimental results deserve further systematic study. As the combination of LIBS and machine learning has become a research hotspot, the CF-LIBS combined with machine learning may lead to its further development. The CF-LIBS based on synthetic spectra can be further promoted and applied due to the progressive perfection of the laser-induced plasma theory and the high development of modern computers. All in all, CF-LIBS is a promising technique for elemental quantitative analysis without standards, promoting the practical applications of LIBS.

Declaration of competing interest

The authors declare that they have no known competing financial interests or personal relationships that could have appeared to influence the work reported in this paper.

Acknowledgments

This research was financially supported by the National Natural Science Foundation of China (No. 62075069).

References

[1] J.D. Winefordner, I.B. Gornushkin, T. Correll, E. Gibb, B.W. Smith, N. Omenetto, Comparing several atomic spectrometric methods to the super stars: special emphasis on laser induced breakdown spectrometry, LIBS, a future super star, J. Anal. At. Spectrom. 19 (2004) 1061–1083.
[2] D.W. Hahn, N. Omenetto, Laser-induced breakdown spectroscopy (LIBS), part I: review of basic diagnostics and plasma–particle interactions: still-challenging issues within the analytical plasma community, Appl. Spectrosc. 64 (2010) 335A–366A.
[3] D.W. Hahn, N. Omenetto, Laser-induced breakdown spectroscopy (LIBS), part II: review of instrumental and methodological approaches to material analysis and applications to different fields, Appl. Spectrosc. 66 (2012) 347–419.
[4] L.-B. Guo, D. Zhang, L.-X. Sun, S.-C. Yao, L. Zhang, Z.-Z. Wang, Q.-Q. Wang, H.-B. Ding, Y. Lu, Z.-Y. Hou, Z. Wang, Development in the application of laser-induced breakdown spectroscopy in recent years: a review, Front. Physiol. 16 (2021).
[5] Z. Wang, M.S. Afgan, W. Gu, Y. Song, Y. Wang, Z. Hou, W. Song, Z. Li, Recent advances in laser-induced breakdown spectroscopy quantification: from fundamental understanding to data processing, Trends Anal. Chem. 143 (2021) 116385.
[6] Z. Wang, Y. Deguchi, F. Shiou, J. Yan, J. Liu, Application of laser-induced breakdown spectroscopy to real-time elemental monitoring of iron and steel making processes, ISIJ Int. 56 (2016) 723–735.
[7] M. Cui, Y. Deguchi, C. Yao, Z. Wang, S. Tanaka, D. Zhang, Carbon detection in solid and liquid steel samples using ultraviolet long-short double pulse laser-induced breakdown spectroscopy, Spectrochim. Acta Part B At. Spectrosc. 167 (2020) 105839.
[8] S. Sheta, M.S. Afgan, Z. Hou, S.-C. Yao, L. Zhang, Z. Li, Z. Wang, Coal analysis by laser-induced breakdown spectroscopy: a tutorial review, J. Anal. At. Spectrom. 34 (2019) 1047–1082.
[9] J. Wu, Y. Qiu, X. Li, H. Yu, Z. Zhang, A. Qiu, Progress of laser-induced breakdown spectroscopy in nuclear industry applications, J. Phys. D Appl. Phys. 53 (2019), 023001.
[10] K. Liu, C. He, C. Zhu, J. Chen, K. Zhan, X. Li, A review of laser-induced breakdown spectroscopy for coal analysis, Trends Anal. Chem. 143 (2021) 116357.
[11] T. Chen, T. Zhang, H. Li, Applications of laser-induced breakdown spectroscopy (LIBS) combined with machine learning in geochemical and environmental resources exploration, Trends Anal. Chem. 133 (2020) 116113.
[12] C. Fabre, Advances in Laser-Induced Breakdown Spectroscopy analysis for geology: a critical review, Spectrochim. Acta Part B At. Spectrosc. 166 (2020) 105799.
[13] R.S. Harmon, G.S. Senesi, Laser-Induced Breakdown Spectroscopy – a geochemical tool for the 21st century, Appl. Geochem. 128 (2021) 104929.
[14] R. Zhou, S. Lin, Y. Ding, H. Yang, K. Ong Yong Keng, M. Hong, Enhancement of laser ablation via interacting spatial double-pulse effect, Opto-Electron. Adv. 1 (2018) 18001401–18001406.
[15] V.N. Lednev, P.A. Sdvizhenskii, R.D. Asyutin, R.S. Tretyakov, M.Y. Grishin, A.Y. Stavertiy, S.M. Pershin, In situ multi-elemental analysis by laser induced breakdown spectroscopy in additive manufacturing, Addit. Manuf. 25 (2019) 64–70.
[16] Y. Ma, Z. Hu, Y. Tang, S. Ma, Y. Chu, X. Li, W. Luo, L. Guo, X. Zeng, Y. Lu, Laser opto-ultrasonic dual detection for simultaneous compositional, structural, and stress analyses for wire + arc additive manufacturing, Addit. Manuf. 31 (2020) 100956.
[17] S. Dittrich, S. Barcikowski, B. Gökce, Plasma and nanoparticle shielding during pulsed laser ablation in liquids cause ablation efficiency decrease, Opto-Electron. Adv. 4 (2021), 200072-200072.
[18] W. Hua-Dong, N.I. Zhi-Bei, F.U. Hong-Bo, J. Jun-Wei, M.W. Sigrist, D. Feng-Zhong, Research and application progress of LIBS in aerosols analysis, J. Atmos. Environ. Optics 11 (2016) 322–337.
[19] Y. Zhang, T. Zhang, H. Li, Application of laser-induced breakdown spectroscopy (LIBS) in environmental monitoring, Spectrochim. Acta Part B At. Spectrosc. 181 (2021) 106218.
[20] B. Busser, S. Moncayo, J.-L. Coll, L. Sancey, V. Motto-Ros, Elemental imaging using laser-induced breakdown spectroscopy: a new and promising approach for biological and medical applications, Coord. Chem. Rev. 358 (2018) 70–79.
[21] S.J. Rehse, A review of the use of laser-induced breakdown spectroscopy for bacterial classification, quantification, and identification, Spectrochim. Acta Part B At. Spectrosc. 154 (2019) 50–69.
[22] Q. Wang, W. Xiangli, G. Teng, X. Cui, K. Wei, A brief review of laser-induced breakdown spectroscopy for human and animal soft tissues: pathological diagnosis and physiological detection, Appl. Spectrosc. Rev. 56 (2020) 221–241.
[23] C. Niu, X. Cheng, T. Zhang, X. Wang, B. He, W. Zhang, Y. Feng, J. Bai, H. Li, Novel method based on hollow laser trapping-LIBS-machine learning for simultaneous quantitative analysis of multiple metal elements in a single microsized particle in air, Anal. Chem. 93 (2021) 2281–2290.
[24] C. Wang, Y.-L. Pan, G. Videen, Optical trapping and laser-spectroscopy measurements of single particles in air: a review, Meas. Sci. Technol. 32 (2021) 102005.

[25] I. Escudero-Sanz, B. Ahlers, G.B. Courreges-Lacoste, Optical design of a combined Raman–laser-induced-breakdown-spectroscopy instrument for the European space agency ExoMars mission, Opt. Eng. 47 (2008), 033001.
[26] R.C. Wiens, S. Maurice, B. Barraclough, M. Saccoccio, W.C. Barkley, J.F. Bell, S. Bender, J. Bernardin, D. Blaney, J. Blank, M. Bouyé, N. Bridges, N. Bultman, P. Caïs, R.C. Clanton, B. Clark, S. Clegg, A. Cousin, D. Cremers, A. Cros, L. DeFlores, D. Delapp, R. Dingler, C. D'Uston, M. Darby Dyar, T. Elliott, D. Enemark, C. Fabre, M. Flores, O. Forni, O. Gasnault, T. Hale, C. Hays, K. Herkenhoff, E. Kan, L. Kirkland, D. Kouach, D. Landis, Y. Langevin, N. Lanza, F. LaRocca, J. Lasue, J. Latino, D. Limonadi, C. Lindensmith, C. Little, N. Mangold, G. Manhes, P. Mauchien, C. McKay, E. Miller, J. Mooney, R.V. Morris, L. Morrison, T. Nelson, H. Newsom, A. Ollila, M. Ott, L. Pares, R. Perez, F. Poitrasson, C. Provost, J.W. Reiter, T. Roberts, F. Romero, V. Sautter, S. Salazar, J.J. Simmonds, R. Stiglich, S. Storms, N. Striebig, J.-J. Thocaven, T. Trujillo, M. Ulibarri, D. Vaniman, N. Warner, R. Waterbury, R. Whitaker, J. Witt, B. Wong-Swanson, The ChemCam instrument suite on the Mars science laboratory (MSL) rover: body unit and combined system tests, Space Sci. Rev. 170 (2012) 167–227.
[27] S. Kubitza, S. Schröder, E. Dietz, S. Frohmann, P.B. Hansen, K. Rammelkamp, D.S. Vogt, M. Gensch, H.-W. Hübers, Detecting sulfur on the Moon: the potential of vacuum ultraviolet laser-induced breakdown spectroscopy, Spectrochim. Acta Part B At. Spectrosc. 174 (2020) 105990.
[28] R.C. Wiens, S. Maurice, S.H. Robinson, A.E. Nelson, P. Cais, P. Bernardi, R.T. Newell, S. Clegg, S.K. Sharma, S. Storms, J. Deming, D. Beckman, A.M. Ollila, O. Gasnault, R.B. Anderson, Y. Andre, S. Michael Angel, G. Arana, E. Auden, P. Beck, J. Becker, K. Benzerara, S. Bernard, O. Beyssac, L. Borges, B. Bousquet, K. Boyd, M. Caffrey, J. Carlson, K. Castro, J. Celis, B. Chide, K. Clark, E. Cloutis, E.C. Cordoba, A. Cousin, M. Dale, L. Deflores, D. Delapp, M. Deleuze, M. Dirmyer, C. Donny, G. Dromart, M. George Duran, M. Egan, J. Ervin, C. Fabre, A. Fau, W. Fischer, O. Forni, T. Fouchet, R. Fresquez, J. Frydenvang, D. Gasway, I. Gontijo, J. Grotzinger, X. Jacob, S. Jacquinod, J.R. Johnson, R.A. Klisiewicz, J. Lake, N. Lanza, J. Laserna, J. Lasue, S. Le Mouelic, C.t. Legett, R. Leveille, E. Lewin, G. Lopez-Reyes, R. Lorenz, E. Lorigny, S.P. Love, B. Lucero, J.M. Madariaga, M. Madsen, S. Madsen, N. Mangold, J.A. Manrique, J.P. Martinez, J. Martinez-Frias, K.P. McCabe, T.H. McConnochie, J.M. McGlown, S.M. McLennan, N. Melikechi, P.Y. Meslin, J.M. Michel, D. Mimoun, A. Misra, G. Montagnac, F. Montmessin, V. Mousset, N. Murdoch, H. Newsom, L.A. Ott, Z.R. Ousnamer, L. Pares, Y. Parot, R. Pawluczyk, C. Glen Peterson, P. Pilleri, P. Pinet, G. Pont, F. Poulet, C. Provost, B. Quertier, H. Quinn, W. Rapin, J.M. Reess, A.H. Regan, A.L. Reyes-Newell, P.J. Romano, C. Royer, F. Rull, B. Sandoval, J.H. Sarrao, V. Sautter, M.J. Schoppers, S. Schroder, D. Seitz, T. Shepherd, P. Sobron, B. Dubois, V. Sridhar, M.J. Toplis, I. Torre-Fdez, I.A. Trettel, M. Underwood, A. Valdez, J. Valdez, D. Venhaus, P. Willis, The SuperCam instrument suite on the NASA Mars 2020 rover: body unit and combined system tests, Space Sci. Rev. 217 (2021) 4.
[29] X. Wan, Design, function, and implementation of China's first LIBS instrument (MarSCoDe) on the Zhurong Mars rover, At. Spectrosc. 42 (2021).
[30] X. Nie, T. Wang, T. Chai, H. Fan, Q. Yu, Application of Laser-Induced Breakdown Spectroscopy in Deep Space Exploration, Second Target Recognition and Artificial Intelligence Summit Forum, SPIE, Changchun, China, 2020, p. 61.
[31] H. Fu, J. Jia, H. Wang, Z. Ni, F. Dong, Calibration Methods of Laser-Induced Breakdown Spectroscopy, Calibration and Validation of Analytical Methods, 2018, pp. 85–107.
[32] V. Costa, D. Babos, J. Castro, D. Andrade, R. Gamela, R. Machado, M. Sperança, A. Araújo, J. Garcia, E. Pereira-Filho, Calibration strategies applied to laser-induced breakdown spectroscopy: a critical review of advances and challenges, J. Braz. Chem. Soc. (2020) 1–13.
[33] W. Xu, C. Sun, Y. Tan, L. Gao, Y. Zhang, Z. Yue, S. Shabbir, M. Wu, L. Zou, F. Chen, S. Liu, J. Yu, Total alkali silica classification of rocks with LIBS: influences of the chemical and physical matrix effects, J. Anal. At. Spectrom. 35 (2020) 1641–1653.
[34] S. Shabbir, Y. Zhang, C. Sun, Z. Yue, W. Xu, L. Zou, F. Chen, J. Yu, Transfer learning improves the prediction performance of a LIBS model for metals with an irregular surface by effectively correcting the physical matrix effect, J. Anal. At. Spectrom. 36 (2021) 1441–1454.
[35] C. Sun, W. Xu, Y. Tan, Y. Zhang, Z. Yue, L. Zou, S. Shabbir, M. Wu, F. Chen, J. Yu, From machine learning to transfer learning in laser-induced breakdown spectroscopy analysis of rocks for Mars exploration, Sci. Rep. 11 (2021) 21379.
[36] X. Li, Z. Wang, Y. Fu, Z. Li, W. Ni, A model combining spectrum standardization and dominant factor based partial least square method for carbon analysis in coal using laser-induced breakdown spectroscopy, Spectrochim. Acta Part B At. Spectrosc. 99 (2014) 82–86.
[37] D. Zhang, H. Zhang, Y. Zhao, Y. Chen, C. Ke, T. Xu, Y. He, A brief review of new data analysis methods of laser-induced breakdown spectroscopy: machine learning, Appl. Spectrosc. Rev. (2020) 1–23.
[38] C. Koral, M. Dell'Aglio, R. Gaudiuso, R. Alrifai, M. Torelli, A. De Giacomo, Nanoparticle-Enhanced Laser Induced Breakdown Spectroscopy for the noninvasive analysis of transparent samples and gemstones, Talanta 182 (2018) 253–258.
[39] M.T. Sweetapple, S. Tassios, Laser-induced breakdown spectroscopy (LIBS) as a tool for in situ mapping and textural interpretation of lithium in pegmatite minerals, Am. Mineral. 100 (2015) 2141–2151.
[40] H.K. Sanghapi, J. Jain, A. Bol'shakov, C. Lopano, D. McIntyre, R. Russo, Determination of elemental composition of shale rocks by laser induced breakdown spectroscopy, Spectrochim. Acta Part B At. Spectrosc. 122 (2016) 9–14.
[41] F. Ruan, T. Zhang, H. Li, Laser-induced breakdown spectroscopy in archeological science: a review of its application and future perspectives, Appl. Spectrosc. Rev. 54 (2019) 573–601.
[42] Y. Gimenez, B. Busser, F. Trichard, A. Kulesza, J.M. Laurent, V. Zaun, F. Lux, J.M. Benoit, G. Panczer, P. Dugourd, O. Tillement, F. Pelascini, L. Sancey, V. Motto-Ros, 3D imaging of nanoparticle distribution in biological tissue by laser-induced breakdown spectroscopy, Sci. Rep. 6 (2016) 29936.
[43] Y. Chu, Z. Zhang, Q. He, F. Chen, Z. Sheng, D. Zhang, H. Jin, F. Jiang, L. Guo, Half-life determination of inorganic-organic hybrid nanomaterials in mice using laser-induced breakdown spectroscopy, J. Adv. Res. 24 (2020) 353–361.
[44] A. Ciucci, M. Corsi, V. Palleschi, S. Rastelli, A. Salvetti, E. Tognoni, New procedure for quantitative elemental analysis by laser-induced plasma spectroscopy, Appl. Spectrosc. 53 (1999) 960–964.
[45] C. Aragon, J.A. Aguilera, Direct analysis of aluminum alloys by CSigma laser-induced breakdown spectroscopy, Anal. Chim. Acta 1009 (2018) 12–19.
[46] Z.Q. Hao, L. Liu, R. Zhou, Y.W. Ma, X.Y. Li, L.B. Guo, Y.F. Lu, X.Y. Zeng, One-point and multi-line calibration method in laser-induced breakdown spectroscopy, Opt Express 26 (2018) 22926–22933.
[47] R. Yuan, Y. Tang, Z. Zhu, Z. Hao, J. Li, H. Yu, Y. Yu, L. Guo, X. Zeng, Y. Lu, Accuracy improvement of quantitative analysis for major elements in laser-induced breakdown spectroscopy using single-sample calibration, Anal. Chim. Acta 1064 (2019) 11–16.
[48] E. Tognoni, G. Cristoforetti, S. Legnaioli, V. Palleschi, Calibration-free laser-induced breakdown spectroscopy: state of the art, Spectrochim. Acta Part B At. Spectrosc. 65 (2010) 1–14.
[49] H. Fu, Z. Ni, H. Wang, J. Jia, F. Dong, Accuracy improvement of calibration-free laser-induced breakdown spectroscopy, Plasma Sci. Technol. 21 (2019), 034001.
[50] A.J. Bauer, S.G. Buckley, Novel applications of laser-induced breakdown spectroscopy, Appl. Spectrosc. 71 (2017) 553–566.
[51] Y. Iida, Effects of atmosphere on laser vaporization and excitation processes of solid samples, Spectrochim. Acta Part B At. Spectrosc. 45 (1990) 1353–1367.
[52] S. Yalçin, D.R. Crosley, G.P. Smith, G.W. Faris, Influence of ambient conditions on the laser air spark, Appl. Phys. B Laser Opt. 68 (1999) 121–130.
[53] A. Kramida, Y. Ralchenko, J. Reader, NIST Atomic Spectra Database, National Institute of Standards and Technology, 2020, Version 5.8.
[54] P.L. Smith, C. Heise, J.R. Esmond, R.L. Kurucz, Atomic Spectral Line Database from CD-ROM 23 of R. L. Kurucz, 2001.
[55] STARK-B Database, http://stark-b.obspm.fr/index.php/home.
[56] S. Messaoud Aberkane, A. Safi, A. Botto, B. Campanella, S. Legnaioli, F. Poggialini, S. Raneri, F. Rezaei, V. Palleschi, Laser-induced breakdown spectroscopy for determination of spectral fundamental parameters, Appl. Sci. 10 (2020) 4973.
[57] E.H. Evans, J. Pisonero, C.M.M. Smith, R.N. Taylor, Atomic spectrometry update: review of advances in atomic spectrometry and related techniques, J. Anal. At. Spectrom. 31 (2016) 1057–1077.
[58] A. Safi, S.H. Tavassoli, G. Cristoforetti, S. Legnaioli, V. Palleschi, F. Rezaei, E. Tognoni, Determination of excitation temperature in laser-induced plasmas using columnar density Saha-Boltzmann plot, J. Adv. Res. 18 (2019) 1–7.
[59] F. Rezaei, G. Cristoforetti, E. Tognoni, S. Legnaioli, V. Palleschi, A. Safi, A review of the current analytical approaches for evaluating, compensating and exploiting self-absorption in Laser Induced Breakdown Spectroscopy, Spectrochim. Acta Part B At. Spectrosc. 169 (2020) 105878.
[60] S. Eliezer, A.D. Krumbein, D. Salzmann, A generalised validity condition for local thermodynamic equilibrium in a laser-produced plasma, J. Phys. D Appl. Phys. 11 (1978) 1693–1701.
[61] Y. Zhang, Z. Zhao, T. Xu, G. Niu, Y. Liu, Y. Duan, Characterization of local thermodynamic equilibrium in a laser-induced aluminum alloy plasma, Appl. Opt. 55 (2016) 2741–2747.
[62] J. Hermann, D. Grojo, E. Axente, V. Craciun, Local thermodynamic equilibrium in a laser-induced plasma evidenced by blackbody radiation, Spectrochim. Acta Part B At. Spectrosc. 144 (2018) 82–86.
[63] E. Tognoni, G. Cristoforetti, S. Legnaioli, V. Palleschi, A. Salvetti, M. Müller, U. Panne, I. Gornushkin, A numerical study of expected accuracy and precision in calibration-free laser-induced breakdown spectroscopy in the assumption of ideal analytical plasma, Spectrochim. Acta Part B At. Spectrosc. 62 (2007) 1287–1302.
[64] A.M. El Sherbini, H. Hegazy, T.M. El Sherbini, Measurement of electron density utilizing the Hα-line from laser produced plasma in air, Spectrochim. Acta Part B At. Spectrosc. 61 (2006) 532–539.
[65] L. Sun, H. Yu, Correction of self-absorption effect in calibration-free laser-induced breakdown spectroscopy by an internal reference method, Talanta 79 (2009) 388–395.
[66] S. Dui-Xiong, S. Mao-Gen, D. Chen-Zhong, W. Xiang-Li, Z. Da-Cheng, M. Xin-Wen, Quantitative analysis of element concentration in Al alloy by using laser-induced breakdown spectroscopy, Acta Phys. Sin. 59 (2010) 4571–4576.

[67] J. Dong, L. Liang, J. Wei, H. Tang, T. Zhang, X. Yang, K. Wang, H. Li, A method for improving the accuracy of calibration-free laser-induced breakdown spectroscopy (CF-LIBS) using determined plasma temperature by genetic algorithm (GA), J. Anal. At. Spectrom. 30 (2015) 1336–1344.
[68] J. Yang, X. Li, J. Xu, X. Ma, A calibration-free laser-induced breakdown spectroscopy (CF-LIBS) quantitative analysis method based on the auto-selection of an internal reference line and optimized estimation of plasma temperature, Appl. Spectrosc. 72 (2018) 129–140.
[69] R. Hai, W. Tong, D. Wu, Z. He, H. Sattar, C. Li, H. Ding, Quantitative analysis of titanium alloys using one-point calibration laser-induced breakdown spectroscopy, Appl. Phys. B Laser Opt. 127 (2021).
[70] T. Li, Z. Hou, Y. Fu, J. Yu, W. Gu, Z. Wang, Correction of self-absorption effect in calibration-free laser-induced breakdown spectroscopy (CF-LIBS) with blackbody radiation reference, Anal. Chim. Acta 1058 (2019) 39–47.
[71] Z. Hu, F. Chen, D. Zhang, Y. Chu, W. Wang, Y. Tang, L. Guo, A method for improving the accuracy of calibration-free laser-induced breakdown spectroscopy by exploiting self-absorption, Anal. Chim. Acta 1183 (2021) 339008.
[72] J.A. Aguilera, C. Aragón, G. Cristoforetti, E. Tognoni, Application of calibration-free laser-induced breakdown spectroscopy to radially resolved spectra from a copper-based alloy laser-induced plasma, Spectrochim. Acta Part B At. Spectrosc. 64 (2009) 685–689.
[73] R.E. Russo, X.L. Mao, J. Yoo, J.J. Gonzalez, Laser Ablation, Laser-Induced Breakdown Spectroscopy, Elsevier, 2007, pp. 41–70.
[74] S.M. Pershin, F. Colao, Laser plasma emission spectrum corrected for the quantitative analysis of alloys, Tech. Phys. Lett. 31 (2005) 741–745.
[75] V.N. Lednev, S.M. Pershin, Plasma stoichiometry correction method in laser-induced breakdown spectroscopy, Laser Phys. 18 (2008) 850–854.
[76] A. Matsumoto, A. Tamura, R. Koda, K. Fukami, Y.H. Ogata, N. Nishi, B. Thornton, T. Sakka, A calibration-free approach for on-site multi-element analysis of metal ions in aqueous solutions by electrodeposition-assisted underwater laser-induced breakdown spectroscopy, Spectrochim. Acta Part B At. Spectrosc. 118 (2016) 45–55.
[77] D. Bulajic, M. Corsi, G. Cristoforetti, S. Legnaioli, V. Palleschi, A. Salvetti, E. Tognoni, A procedure for correcting self-absorption in calibration free-laser induced breakdown spectroscopy, Spectrochim. Acta Part B At. Spectrosc. 57 (2002) 339–353.
[78] R. Ladenburg, F. Reiche, Über selektive absorption, Ann. Phys. 347 (1913) 181–209.
[79] I.B. Gornushkin, J.M. Anzano, L.A. King, B.W. Smith, N. Omenetto, J.D. Winefordner, Curve of growth methodology applied to laser-induced plasma emission spectroscopy, Spectrochim. Acta Part B At. Spectrosc. 54 (1999) 491–503.
[80] A. De Giacomo, M. Dell'Aglio, O. De Pascale, R. Gaudiuso, R. Teghil, A. Santagata, G.P. Parisi, ns- and fs-LIBS of copper-based-alloys: a different approach, Appl. Surf. Sci. 253 (2007) 7677–7681.
[81] R. Gaudiuso, M. Dell'Aglio, O. De Pascale, A. Santagata, A. De Giacomo, Laser-induced plasma analysis of copper alloys based on Local Thermodynamic Equilibrium: an alternative approach to plasma temperature determination and archeometric applications, Spectrochim. Acta Part B At. Spectrosc. 74–75 (2012) 38–45.
[82] G.H. Cavalcanti, D.V. Teixeira, S. Legnaioli, G. Lorenzetti, L. Pardini, V. Palleschi, One-point calibration for calibration-free laser-induced breakdown spectroscopy quantitative analysis, Spectrochim. Acta Part B At. Spectrosc. 87 (2013) 51–56.
[83] L.C.L. Borduchi, D.M.B.P. Milori, P.R. Villas-Boas, One-point calibration of Saha-Boltzmann plot to improve accuracy and precision of quantitative analysis using laser-induced breakdown spectroscopy, Spectrochim. Acta Part B At. Spectrosc. 160 (2019) 105692.
[84] H. Fu, F. Dong, H. Wang, J. Jia, Z. Ni, Calibration-free laser-induced breakdown spectroscopy (CF-LIBS) with standard reference line for the analysis of stainless steel, Appl. Spectrosc. 71 (2017) 1982–1989.
[85] H. Fu, H. Wang, J. Jia, Z. Ni, F. Dong, Standard reference line combined with one-point calibration-free laser-induced breakdown spectroscopy (CF-LIBS) to quantitatively analyze stainless and heat resistant steel, Appl. Spectrosc. 72 (2018) 1183–1188.
[86] E. D'Andrea, S. Pagnotta, E. Grifoni, S. Legnaioli, G. Lorenzetti, V. Palleschi, B. Lazzerini, A hybrid calibration-free/artificial neural networks approach to the quantitative analysis of LIBS spectra, Appl. Phys. B Laser Opt. 118 (2015) 353–360.
[87] I.B. Gornushkin, A.Y. Kazakov, N. Omenetto, B.W. Smith, J.D. Winefordner, Radiation dynamics of post-breakdown laser induced plasma, Spectrochim. Acta Part B At. Spectrosc. 59 (2004) 401–418.
[88] I.B. Gornushkin, A.Y. Kazakov, N. Omenetto, B.W. Smith, J.D. Winefordner, Experimental verification of a radiative model of laser-induced plasma expanding into vacuum, Spectrochim. Acta Part B At. Spectrosc. 60 (2005) 215–230.
[89] P. Yaroshchyk, D. Body, R.J.S. Morrison, B.L. Chadwick, A semi-quantitative standard-less analysis method for laser-induced breakdown spectroscopy, Spectrochim. Acta Part B At. Spectrosc. 61 (2006) 200–209.
[90] A. Demidov, S. Eschlböck-Fuchs, A.Y. Kazakov, I.B. Gornushkin, P.J. Kolmhofer, J.D. Pedarnig, N. Huber, J. Heitz, T. Schmid, R. Rössler, U. Panne, Monte Carlo standardless approach for laser induced breakdown spectroscopy based on massive parallel graphic processing unit computing, Spectrochim. Acta Part B At. Spectrosc. 125 (2016) 97–102.
[91] P. Kumar, R.K. Kushawaha, S.B. Banerjee, K.P. Subramanian, N.G. Rudraswami, Quantitative estimation of elemental composition employing a synthetic generated spectrum, Appl. Opt. 57 (2018) 5443–5450.
[92] G. Cristoforetti, E. Tognoni, Calculation of elemental columnar density from self-absorbed lines in laser-induced breakdown spectroscopy: a resource for quantitative analysis, Spectrochim. Acta Part B At. Spectrosc. 79–80 (2013) 63–71.
[93] Q. Abbass, N. Ahmed, R. Ahmed, M.A. Baig, A comparative study of calibration free methods for the elemental analysis by laser induced breakdown spectroscopy, Plasma Chem. Plasma Process. 36 (2016) 1287–1299.
[94] M.L. Shah, A.K. Pulhani, G.P. Gupta, B.M. Suri, Quantitative elemental analysis of steel using calibration-free laser-induced breakdown spectroscopy, Appl. Opt. 51 (2012) 4612–4621.
[95] P.J. Kolmhofer, S. Eschlböck-Fuchs, N. Huber, R. Rössler, J. Heitz, J.D. Pedarnig, Calibration-free analysis of steel slag by laser-induced breakdown spectroscopy with combined UV and VIS spectra, Spectrochim. Acta Part B At. Spectrosc. 106 (2015) 67–74.
[96] D. Zhu, Y. Cao, R. Zhong, X. Chen, Quantitative analysis of composition change in AZ31 magnesium alloy using CF-LIBS after laser material processing, Plasma Sci. Technol. 17 (2015) 909–913.
[97] H. Shakeel, S.U. Haq, G. Aisha, A. Nadeem, Quantitative analysis of Al-Si alloy using calibration free laser induced breakdown spectroscopy (CF-LIBS), Phys. Plasmas 24 (2017), 063516.
[98] I. Urbina, D. Carneiro, S. Rocha, E.E. Farias, F. Bredice, V. Palleschi, Study of binary lead-tin alloys using a new procedure based on calibration-free laser induced breakdown spectroscopy, Spectrochim. Acta Part B At. Spectrosc. 170 (2020) 105902.
[99] F. Colao, R. Fantoni, V. Lazic, A. Paolini, F. Fabbri, G.G. Ori, L. Marinangeli, A. Baliva, Investigation of LIBS feasibility for in situ planetary exploration: an analysis on Martian rock analogues, Planet. Space Sci. 52 (2004) 117–123.
[100] G.S. Senesi, G. Tempesta, P. Manzari, G. Agrosì, An innovative approach to meteorite analysis by laser-induced breakdown spectroscopy, Geostand. Geoanal. Res. 40 (2016) 533–541.
[101] M. Dell'Aglio, M. López-Claros, J.J. Laserna, S. Longo, A. De Giacomo, Stand-off laser induced breakdown spectroscopy on meteorites: calibration-free approach, Spectrochim. Acta Part B At. Spectrosc. 147 (2018) 87–92.
[102] M. Fahad, Z. Farooq, M. Abrar, Comparative study of calibration-free laser-induced breakdown spectroscopy methods for quantitative elemental analysis of quartz-bearing limestone, Appl. Opt. 58 (2019) 3501–3508.
[103] M. Fahad, S. Ali, K.H. Shah, A. Shahzad, M. Abrar, Quantitative elemental analysis of high silica bauxite using calibration-free laser-induced breakdown spectroscopy, Appl. Opt. 58 (2019) 7588–7596.
[104] M. Fahad, A. Shahzad, S. Ali, K.H. Shah, Qualitative and quantitative analysis of steatite using calibration-free laser-induced breakdown spectroscopy in conjunction with x-ray fluorescence spectroscopy and Fourier-transform infrared spectroscopy, Appl. Opt. 60 (2021) 5110–5116.
[105] T.F. Akhmetzhanov, T.A. Labutin, S.M. Zaytsev, A.N. Drozdova, A.M. Popov, Determination of the Mn/Fe ratio in ferromanganese nodules using calibration-free laser-induced breakdown spectroscopy, Opt Spectrosc. 126 (2019) 316–320.
[106] A. Ahmad, M. Hafeez, S.A. Abbasi, T.M. Khan, M.R.I. Faruque, M.U. Khandaker, P. Ahmad, M. Rafique, N. Haleem, Compositional analysis of chalcopyrite using calibration-free laser-induced breakdown spectroscopy, Appl. Sci. 10 (2020) 6848.
[107] M. Hafeez, S.A. Abbasi, M. Rafique, R. Hayder, M. Sajid, J. Iqbal, N. Ahmad, S. Shahida, Calibration-free laser-induced breakdown spectroscopic analysis of copper-rich mineral collected from the Gilgit-Baltistan region of Pakistan, Appl. Opt. 59 (2020) 68–76.
[108] J.M. Anzano, A. Cruz-Conesa, R.J. Lasheras, C. Marina-Montes, L.V. Pérez-Arribas, J.O. Cáceres, A.I. Velásquez, V. Palleschi, Multielemental analysis of Antarctic soils using calibration free laser-induced breakdown spectroscopy, Spectrochim. Acta Part B At. Spectrosc. 180 (2021) 106191.
[109] I. Borgia, L.M.F. Burgio, M. Corsi, R. Fantoni, V. Palleschi, A. Salvetti, M.C. Squarcialupi, E. Tognoni, Self-calibrated quantitative elemental analysis by laser-induced plasma spectroscopy: application to pigment analysis, J. Cult. Herit. 1 (2000) S281–S286.
[110] M. Bicchieri, M. Nardone, P.A. Russo, A. Sodo, M. Corsi, G. Cristoforetti, V. Palleschi, A. Salvetti, E. Tognoni, Characterization of azurite and lazurite based pigments by laser induced breakdown spectroscopy and micro-Raman spectroscopy, Spectrochim. Acta Part B At. Spectrosc. 56 (2001) 915–922.
[111] M. Corsi, G. Cristoforetti, M. Giuffrida, M. Hidalgo, S. Legnaioli, L. Masotti, V. Palleschi, A. Salvetti, E. Tognoni, C. Vallebona, Archaeometric analysis of ancient copper artefacts by laser-induced breakdown spectroscopy technique, Microchim. Acta 152 (2005) 105–111.
[112] G.S. Senesi, D. Manzini, O. De Pascale, Application of a laser-induced breakdown spectroscopy handheld instrument to the diagnostic analysis of stone monuments, Appl. Geochem. 96 (2018) 87–91.
[113] M. Corsi, G. Cristoforetti, M. Hidalgo, S. Legnaioli, V. Palleschi, A. Salvetti, E. Tognoni, C. Vallebona, Application of laser-induced breakdown spectroscopy technique to hair tissue mineral analysis, Appl. Opt. 42 (2003) 6133–6137.
[114] S. Pandhija, A.K. Rai, In situ multielemental monitoring in coral skeleton by CF-LIBS, Appl. Phys. B Laser Opt. 94 (2009) 545–552.

[115] V.K. Singh, V. Singh, A.K. Rai, S.N. Thakur, P.K. Rai, J.P. Singh, Quantitative analysis of gallstones using laser-induced breakdown spectroscopy, Appl. Opt. 47 (2008) G38–G47.
[116] J. Iqbal, H. Asghar, S.K.H. Shah, M. Naeem, S.A. Abbasi, R. Ali, Elemental analysis of sage (herb) using calibration-free laser-induced breakdown spectroscopy, Appl. Opt. 59 (2020) 4927–4932.
[117] A. Marín Roldán, V. Dwivedi, J. Yravedra Sainz de los Terreros, P. Veis, Laser-Induced breakdown spectroscopy (LIBS) for the analyses of faunal bones: assembling of individuals and elemental quantification, Optik 218 (2020) 164992.
[118] M. Al-Salihi, R. Yi, S. Wang, Q. Wu, F. Lin, J. Qu, L. Liu, Quantitative laser-induced breakdown spectroscopy for discriminating neoplastic tissues from non-neoplastic ones, Opt Express 29 (2021) 4159–4173.
[119] S. Zhang, Z. Hu, Z. Zhao, F. Chen, Y. Tang, Z. Sheng, D. Zhang, Z. Zhang, H. Jin, H. Pu, L. Guo, Quantitative analysis of mineral elements in hair and nails using calibration-free laser-induced breakdown spectroscopy, Optik 242 (2021) 167067.
[120] V.S. Burakov, S.N. Raikov, Quantitative analysis of alloys and glasses by a calibration-free method using laser-induced breakdown spectroscopy, Spectrochim. Acta Part B At. Spectrosc. 62 (2007) 217–223.
[121] B. Praher, V. Palleschi, R. Viskup, J. Heitz, J.D. Pedarnig, Calibration free laser-induced breakdown spectroscopy of oxide materials, Spectrochim. Acta Part B At. Spectrosc. 65 (2010) 671–679.
[122] J.D. Pedarnig, P. Kolmhofer, N. Huber, B. Praher, J. Heitz, R. Rössler, Element analysis of complex materials by calibration-free laser-induced breakdown spectroscopy, Appl. Phys. Mater. Sci. Process 112 (2012) 105–111.
[123] S.A. Davari, S. Hu, D. Mukherjee, Calibration-free quantitative analysis of elemental ratios in intermetallic nanoalloys and nanocomposites using Laser Induced Breakdown Spectroscopy (LIBS), Talanta 164 (2017) 330–340.
[124] S.A. Davari, S. Hu, R. Pamu, D. Mukherjee, Calibration-free quantitative analysis of thin-film oxide layers in semiconductors using laser induced breakdown spectroscopy (LIBS), J. Anal. At. Spectrom. 32 (2017) 1378–1387.
[125] S. Pagnotta, M. Lezzerini, B. Campanella, G. Gallello, E. Grifoni, S. Legnaioli, G. Lorenzetti, F. Poggialini, S. Raneri, A. Safi, V. Palleschi, Fast quantitative elemental mapping of highly inhomogeneous materials by micro-Laser-Induced Breakdown Spectroscopy, Spectrochim. Acta Part B At. Spectrosc. 146 (2018) 9–15.
[126] J. Hermann, A. Lorusso, A. Perrone, F. Strafella, C. Dutouquet, B. Torralba, Simulation of emission spectra from nonuniform reactive laser-induced plasmas, Phys. Rev. E: Stat., Nonlinear, Soft Matter Phys. 92 (2015), 053103.
[127] J. Hermann, E. Axente, F. Pelascini, V. Craciun, Analysis of multi-elemental thin films via calibration-free laser-induced breakdown spectroscopy, Anal. Chem. 91 (2019) 2544–2550.
[128] Z. Farooq, R. Ali, A. Ali, T. Mubeen, T. Jan, H. Anwar, Calibration-free laser-induced plasma analysis of nanoparticle-doped material using self-absorption correction methodologies, Appl. Spectrosc. 73 (2019) 30–39.
[129] H. Shakeel, S.U. Haq, V. Contreras, Q. Abbas, A. Nadeem, Analysis of alloy and solar cells with double-pulse calibration-free laser-induced breakdown spectroscopy, Optik 211 (2020) 164627.
[130] C. Gerhard, A. Taleb, F. Pelascini, J. Hermann, Quantification of surface contamination on optical glass via sensitivity-improved calibration-free laser-induced breakdown spectroscopy, Appl. Surf. Sci. 537 (2021) 147984.
[131] M. Corsi, V. Palleschi, A. Salvetti, E. Tognoni, Calibration free laser induced plasma spectroscopy: a new method for combustion products analysis, Clean. Air 3 (2002) 69–79.
[132] M. Corsi, G. Cristoforetti, M. Hidalgo, S. Legnaioli, V. Palleschi, A. Salvetti, E. Tognoni, C. Vallebona, Double pulse, calibration-free laser-induced breakdown spectroscopy: a new technique for in situ standard-less analysis of polluted soils, Appl. Geochem. 21 (2006) 748–755.
[133] R. Kumar, A.K. Rai, D. Alamelu, S.K. Aggarwal, Monitoring of toxic elements present in sludge of industrial waste using CF-LIBS, Environ. Monit. Assess. 185 (2013) 171–180.
[134] M. Boudhib, J. Hermann, C. Dutouquet, Compositional analysis of aerosols using calibration-free laser-induced breakdown spectroscopy, Anal. Chem. 88 (2016) 4029–4035.
[135] M. Akhtar, A. Jabbar, S. Mahmood, Z.A. Umar, R. Ahmed, M. Aslam Baig, Analysis of soil by magnetic field assisted calibration-free laser induced breakdown spectroscopy (CF-LIBS) and laser ablation – time-of-flight mass spectrometry (LA-TOF-MS), Anal. Lett. 52 (2019) 2312–2328.
[136] V. Contreras, M.A. Meneses-Nava, O. Barbosa-García, J.L. Maldonado, G. Ramos-Ortiz, Double-pulse and calibration-free laser-induced breakdown spectroscopy at low-ablative energies, Opt. Lett. 37 (2012) 4591–4593.
[137] A. Marín Roldán, M. Pisarčík, M. Veis, M. Držík, P. Veis, Calibration-free analysis of a tungsten-based target for diagnostics of relevant fusion materials comparing picosecond and nanosecond LIBS, Spectrochim. Acta Part B At. Spectrosc. 177 (2021) 106055.